

Acoustic Studies of AC Conductivity Mechanisms in n -GaAs/AlGaAs in the Integer and Fractional Quantum Hall Effect Regime.

I.L. Drichko,¹ I.Yu. Smirnov,^{1,*} A.V. Suslov,² and D.R. Leadley³

¹*A.F. Ioffe Physical-Technical Institute of Russian Academy of Sciences, 194021 St. Petersburg, Russia*

²*National High Magnetic Field Laboratory, Tallahassee, FL 32310, USA*

³*Department of Physics, University of Warwick, Coventry CV4 7AL, UK*

(Dated: September 11, 2022)

In case of a of the heterostructure n -GaAs/AlGaAs with sheet density $n = 2 \times 10^{11} \text{cm}^{-2}$ and mobility $\mu \approx 2 \times 10^6 \text{cm}^2/\text{V}\cdot\text{s}$ with integer and fractional quantum Hall effect (IQHE and FQHE, respectively) we demonstrate the wide applicability of acoustic methods for determining the general conduction parameters of a two dimensional electron gas. We also examine the mechanisms of low-temperature conductivity in the minima of oscillations of high frequency conductivity in the IQHE and FQHE regimes. In the magnetic field region where electrons are delocalized, the parameters determined by the acoustic technique do not differ from those determined by a direct current. However, the acoustic measurements do not require Hall bars and electrical contacts to be fabricated. In the minima of IQHE and FQHE oscillations electrons are localized, and ac conductivity turns to be via hopping. An analysis of the high frequency conductivity in the QHE regime has been carried out within a "two site" model. Furthermore, measurements of acoustoelectric effects in a tilted magnetic field provided the dependence of the activation energy on magnetic field in the fractional quantum Hall effect regime at $\nu=2/3$.

PACS numbers: 73.23.-b, 73.43.Qt

I. INTRODUCTION

Electrons in modulation-doped GaAs/AlGaAs have been recorded with a mobility of over $10^7 \text{cm}^2/\text{V}\cdot\text{s}$, which has attracted huge interest from experimentalists engaged with the physics of two-dimensional systems. Indeed, amazing features such as the integer and fractional quantum Hall effects¹ have been discovered, leading to two Nobel Prizes, and the properties of these structures have been studied by numerous authors with various methods.

In our studies, we use contactless acoustic methods to investigate the quantum Hall effect in n -GaAs/AlGaAs heterostructures, grown by molecular beam epitaxy. This technique was first employed experimentally in Ref. 2, with theoretical calculations of the absorption coefficient and velocity of a surface acoustic wave (SAW) interacting with the carriers in the two dimensional channel made in Ref. 3. The aim of the present paper is to demonstrate how the kinetic characteristics of delocalized electrons, as well as features of low-temperature hopping conduction, can be determined by this method using the example of a n -GaAs/AlGaAs heterostructure with an electron mobility $\mu \approx 2 \times 10^6 \text{cm}^2/\text{V}\cdot\text{s}$ and a carrier concentration of $n = 2 \times 10^{11} \text{cm}^{-2}$. For well studied materials, such as n -GaAs/AlGaAs, the techniques required to manufacture Hall-bar samples with ohmic contacts is well established, which means that the material parameters can be reliably obtained from direct current measurements. However, for a number of new systems, where the quality of the contacts can be a serious problem, acoustic methods provide an option to analyze the material parameters in a contactless way, requiring only samples in a standard rectangular form of a plate with macroscopic

dimensions of $\approx 5 \text{mm} \times 5 \text{mm}$. Although there have been numerous previous excellent studies of SAW effects in GaAs heterojunctions, we will discuss here how the technique can be used more generally as a substitute for contact measurements in extracting numerical parameters of electrons/holes at the low dimensional interface. This implementation was realized for the first time.

In a magnetic field, the SAW absorption and velocity show Shubnikov-de Haas (SdH)-type oscillations. Although the acoustic measurements are relative, the absolute characteristics of the delocalized carriers (an electron gas): the carrier concentration, mobility, conductivity at zero magnetic field, and the transport relaxation time, can be determined in the linear regime. In the nonlinear regime, when the ac conductivity begins to depend on the SAW intensity, one can also determine the energy relaxation time.⁴ Our experimental configuration, which we refer to as "hybrid", opens up the possibility to not only explore materials that lack an inversion center, such as $A^{\text{III}}B^{\text{V}}$, but also those with an inversion center, e.g. Ge, Si etc. Nevertheless, to obtain the numerical data of material parameters in the hybrid experimental configuration it is necessary to determine the gap between the sample and the lithium niobate platelet, which is formed due to the roughness of both surfaces. We have developed methods to determine this gap for the first time.

Within the quantum Hall effect regime, it is usual for researchers using acoustic methods to compare the observed experimental dependences of the SAW attenuation on the magnetic field with the conductivity measured with a direct current. We have shown that it is not quite correct. In the quantum Hall minima (of the SdH resistance oscillations and oscillations of the SAW absorption and velocity) the conductivity has a hopping

nature and in the hopping regime the high frequency (ac) and dc conductivities have different mechanisms: While dc-conductivity is realized by hopping of carriers between centers that are close in *energy* (variable range hopping regime) from one end of the sample to the other, the ac conductivity is due to hopping between two *spatially* close sites and has a complex form $\sigma^{ac} = \sigma_1 - i\sigma_2$ for the 2-dimensional case.⁵ We have developed a technique to determine the real and imaginary components of the conductivity by simultaneous measurements of the magnetic field dependences of the SAW attenuation and velocity,⁶ which is particularly powerful since determination of the imaginary part of the hopping conductivity at high frequency measurements is usually troublesome.

When the charge carriers are delocalized, in the SAW frequency range employed in this work, the imaginary component of conductivity is very small and can be neglected $\sigma_1 > \sigma_2 \approx 0$, thus $\sigma^{ac} = \sigma^{dc}$; however, if the carriers are localized and conductivity is of a hopping nature the imaginary component of conductivity can exceed the real one $\sigma_2 > \sigma_1$.⁵ In the integer quantum Hall effect (IQHE) regime, the high frequency conductivity oscillation minima corresponds to the carriers being completely or partially localized. In latter case, the conductivity mechanism is a mixture of hopping via localized states and conduction of delocalized electrons through the extended states. The ratio of the real and imaginary components of the ac conductivity then gives a qualitative indication of the fraction of localized charge carriers. Such an analysis was carried out for the first time.

The fractional quantum Hall effect (FQHE) regime has also been the subject of detailed studies by a very large number of researchers.⁷ An extensive study of the FQHE by acoustic methods has also been performed and is reviewed in Ref. 8. However, much of this survey focused on an analysis of the magnetic field region close to filling factor $\nu=1/2$, i.e., the one used to argue theoretically the existence of composite fermions (CFs).⁹ The dispersion of excitations in the fractional Hall effect regime, using high-frequency SAWs, was studied in Ref. 10.

In our study, we investigated the ac conductivity by acoustic methods at filling factor $\nu=2/3$, which falls at $B \approx 12$ T in our sample. The FQHE at $\nu=2/3$ is of great interest, because in the CF model this state consists of two filled CF Landau levels (LLs) and so can be either unpolarized, at low Zeeman energy, or fully spin polarized at higher Zeeman energy. The spin transition between these states has been investigated by tilting the sample in a magnetic field to increase the total magnetic field (setting the Zeeman energy) for a given perpendicular component (that determines the filling factor).¹¹⁻¹⁴ As an alternative the Zeeman energy can be reduced, all the way to zero, by using hydrostatic pressure to alter the band structure.^{15,16} However, in many of the tilted magnetic field studies,¹⁷⁻²⁰ the carrier concentration in the sample was too high to directly observe the paramagnetic-ferromagnetic transition at $\nu=2/3$ associated with the crossing of the CF Landau levels, as is also the case for

our sample. Instead these studies measured the magnetic field dependence of the activation energy on the ferromagnetic side. It is assumed that, based on a simple model of composite fermions, the energy gap in the FQHE regime should be determined by the Coulomb interaction in the form $\Delta E \propto e^2/\epsilon l_B$, where $l_B = \sqrt{\hbar c/eB}$ is the magnetic length, and therefore $\Delta E \propto \sqrt{B}$.

However, this dependence was not observed in any of the above tilted field experiments. Furthermore, in the pressure experiments it was observed that the CF energy gap scaled like $\sqrt{B^*}$, where $B^* = B - 2(h/e)n$ is the effective magnetic field in which the CF moves,¹⁵ as might be expected given the fractal nature of the QHE.²¹ Therefore, it is useful to also determine the dependence of $\Delta E(B)$ by acoustic contactless methods. A study of the FQHE using acoustic methods at $\nu=2/3$ was implemented in Ref. 22, motivated by the conclusion from dc measurements that domains are formed in the vicinity of the spin transition, to determine the width of these domain walls. However, in the frequency range 100 MHz - 2 GHz no effects on the SAW propagation have been observed in the spin transition region.

In addition to the above mentioned aims, the purpose of our present work is to determine the conductivity mechanism for electrons in FQHE regime ($\nu=2/3$) in a fully spin-polarized - ferromagnetic region and to determine the dependence of the energy gap of this state on the magnetic field in one more way, by measuring the high-frequency conductivity acoustically.

II. EXPERIMENTAL METHOD

The complex high frequency conductivity $\sigma^{ac} \equiv \sigma_1 - i\sigma_2$ was investigated in a *n*-GaAs/AlGaAs sample, over the temperature range 0.3-4.2 K and with a perpendicular and tilted magnetic field of up to 18 T. The sample had a carrier concentration of $n \approx 2 \times 10^{11} \text{ cm}^{-2}$ and mobility $\mu \approx 2 \times 10^6 \text{ cm}^2/\text{V}\cdot\text{s}$, as obtained from dc transport measurements in the dark. This investigation used acoustic methods to measure the absorption of a SAW Γ and it's velocity shift in magnetic field - $\Delta v(B)/v(0)$. The SAW frequency was varied from 30 to 254 MHz.

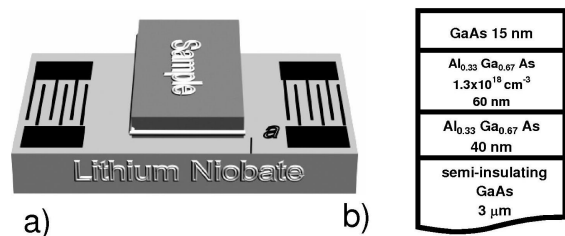


FIG. 1. Sketches of the (a) acoustic experiment setup and (b) sample.

Acoustic methods, based on the use of a surface acoustic wave, provide an opportunity to work with samples of a square or rectangular shape without fabricating electrical contacts, which can otherwise plague the interpretation of dc transport measurements at low temperature. For this purpose the "hybrid" method was used, whereby the SAW, excited by interdigital transducers, propagates along the surface of the piezoelectric lithium niobate, and the structure to be studied is slightly pressed onto the surface of the LiNbO₃ substrate by means of springs (shown in Fig. 1 a). The acoustic deformation wave, propagating along the surface of the LiNbO₃, is accompanied by a wave of electric field with the same frequency. This electric field penetrates into the 2D channel of the GaAs sample, exciting high-frequency currents, which in turn lead to absorption of the wave energy. Interaction of the SAW electric field with the electrons in a quantum well also results in a shift of the SAW velocity. In this experimental configuration, the strain is not transmitted to the studied system due to an effective clearance between the sample and niobate.⁶

From the experimentally measured values of the SAW absorption $\Delta\Gamma = \Gamma(B) - \Gamma(0)$ and the relative change of the SAW velocity $\Delta v/v = (v(B) - v(0))/v(0)$ in a magnetic field one can calculate the real σ_1 and imaginary σ_2 components of high-frequency conductivity using the equations (1) and (2).³ Since $\Gamma(B=0) \ll \Gamma(B)$:

$$\Gamma = 8.68 \frac{K^2}{2} qA \times \frac{4\pi\sigma_1 t(q)/\varepsilon_s v}{[1 + 4\pi\sigma_2 t(q)/\varepsilon_s v]^2 + [4\pi\sigma_1 t(q)/\varepsilon_s v]^2}, \text{ dB/cm} \quad (1)$$

where $A = 8b(q)(\varepsilon_1 + \varepsilon_0)\varepsilon_0^2\varepsilon_s \exp[-2q(a+d)]$, and

$$\frac{\Delta v}{v} = \frac{K^2}{2} A \times \frac{1 + 4\pi\sigma_2 t(q)/\varepsilon_s v}{[1 + 4\pi\sigma_2 t(q)/\varepsilon_s v]^2 + [4\pi\sigma_1 t(q)/\varepsilon_s v]^2}, \quad (2)$$

where K^2 is the electro-mechanic coupling constant for lithium niobate (Y-cut in our experiments), q and v are the SAW wave vector and velocity in LiNbO₃, respectively; a is the gap between the piezoelectric plate and the sample, d is the distance between the sample surface and the 2DEG layer; ε_1 , ε_0 and ε_s are the dielectric constants of LiNbO₃, of vacuum, and of the semiconductor, respectively; $b(q)$ and $t(q)$ are complex functions of a , d , ε_1 , ε_0 and ε_s given in Ref. 3. Using these equations one may obtain σ_1 and σ_2 provided that the values of a and d are known. The technological process of sample production determines d , and a is a fitting parameter which is determined in an appropriate way for the effect being studied (see below). This value depends both on the procedure of mounting the sample on the lithium niobate surface as well as on the quality of sample and niobate surfaces.

The modulation doped GaAs heterostructure (shown in Fig. 1 b) was grown by molecular beam epitaxy at Philips Redhill²³ starting from a semi-insulating GaAs

substrate with $3\mu\text{m}$ of epitaxial GaAs forming the conducting channel where the two dimensional electron gas (2DEG) is located, followed by a 40 nm undoped Al_{0.33}Ga_{0.67}As spacer layer followed by a 60 nm supply layer of Al_{0.33}Ga_{0.67}As doped with a Si donor concentration at $1.3 \times 10^{18} \text{ cm}^{-3}$, and finally a 15 nm GaAs cap.

III. EXPERIMENTAL RESULTS AND DISCUSSION

A. Linear regime

We will first discuss the results obtained in the linear regime where the response does not depend on the input SAW power. For this section the output from the RF generator was kept below $1 \mu\text{W}$. Fig. 2 shows the magnetic field dependence of the attenuation Γ and the SAW velocity change $\Delta v/v(0)$ at different temperatures from 0.3 K to 4.2 K using a SAW frequency of $f=30 \text{ MHz}$.

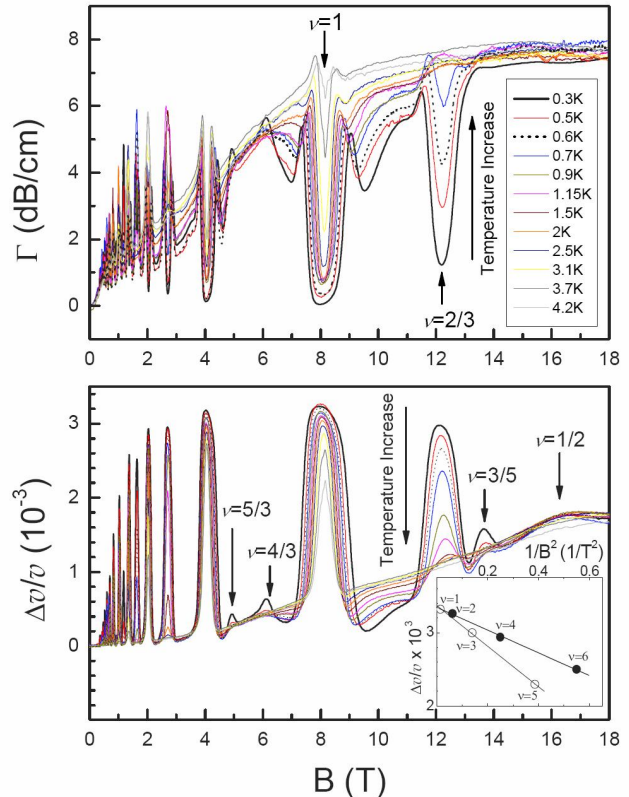


FIG. 2. (Color online) Magnetic field dependences of the ultrasound attenuation Γ and velocity shift $\Delta v/v(0)$ for different temperatures; $v(0) \approx 3.5 \times 10^5 \text{ cm/s}$ is the zero-field SAW velocity; $f = 30 \text{ MHz}$. Inset: the dependence of the maxima $\Delta v/v$ on $1/B^2$ for odd and even filling factors; $f = 30 \text{ MHz}$, $T=0.3 \text{ K}$; lines are results of the linear fit.

One can see that magnetic field induces oscillations of the absorption coefficient and the velocity change, anal-

ogous to the SdH oscillations seen in ρ_{xx} when using a direct current. These extrema vary with temperature much like SdH oscillations with the odd integer features disappearing faster with increasing temperature than the even integer features. In addition FQHE features can be seen near to filling factor $2/3$ and weaker ones $5/3$, $4/3$ and $3/5$ as well as the temperature independent point at $1/2$.

According to Eq.2, the value of $\Delta v/v$ should increase as $1/B^2$ and saturate at the value $K^2A/2$ in a strong magnetic field. Such behavior is seen in Fig. 2, where the maximum value at different ν does tend to saturate. Furthermore, if we construct the dependence (see inset of Fig. 2) of the maxima $\Delta v/v$ on $1/B^2$ separately for odd filling factors 1,3,5... and even filling factors 2,4,6... we obtain two straight lines, with different slopes, which intersect at $1/B^2=0$. This intersection is equal to the saturation value, from which we can deduce the empirical parameter a , $a \approx (0.8 - 1.0) \times 10^{-4}$ cm.

Having found a , we can now calculate the conductivity σ_1 and σ_2 from the measured Γ and $\Delta v/v(0)$ by using equations (1) and (2).

The dependence of the real part of the ac conductivity in the two-dimensional channel σ_1 on the magnetic field, derived from the curves in Fig. 2 is represented in Fig. 3, where it can be seen that σ_1 changes by 5 orders of magnitude, from 10^{-4} at low field to $\approx 10^{-9}$ Ohm $^{-1}$ in the minima of the SdH oscillation. Naturally, the high conductivity in weak magnetic fields and low conductivity in the oscillation minima is implemented by different mechanisms. Therefore, we will consider the mechanisms of conductivity for the different regions separately and show the feasibility of using acoustic methods to determine the parameters of the material under these different conditions.

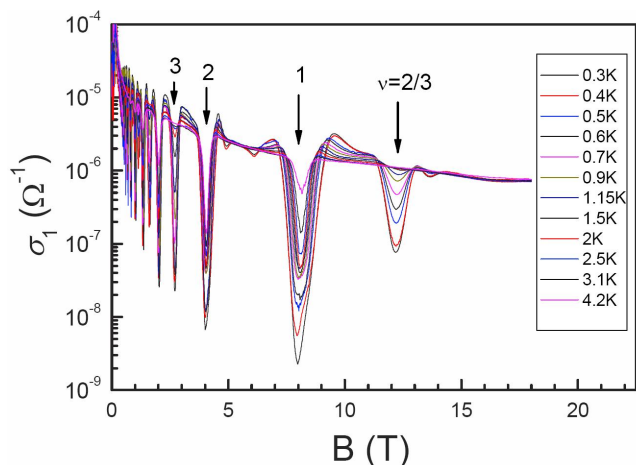


FIG. 3. (Color online) Magnetic field dependence of the real part of the ac conductivity σ_1 at temperatures from 0.3 K to 4.2 K; $f=30$ MHz.

1. Regime of the free charge carriers, $B < 1$ T

Measurements of the SAW absorption coefficient Γ and velocity shift $\Delta v(B)/v(0)$ are relative, since they are usually carried out by changing some external impact (magnetic or electric field, irradiation, etc.). Hence, it is impossible to directly determine the absolute values of conductivity, or the mobility of charge carriers at $B=0$ from these measurements. However, these parameters can be found in high mobility samples, which exhibit many SdH oscillations in relatively small magnetic fields, where the charge carriers are delocalized and the dc conductivity $\sigma^{dc} = \sigma_1 \gg \sigma_2 \approx 0$. In accordance with Ref. 24:

$$\sigma_{xx} = \sigma_{xx}^* + \sigma_{xx}^{osc}$$

$$\sigma_{xx}^* = \frac{\sigma_0}{1 + \omega_c^2 \tau_0^2} = \frac{enc^2}{\mu B^2}, \text{ provided } (\omega_c^2 \tau_0^2) \gg 1 \quad (3)$$

where σ_0 is the zero magnetic field conductivity, $\omega_c = eB/m^*c$ is the cyclotron frequency, τ_0 is the transport relaxation time; $c=3 \times 10^{10}$ cm/s, e is the electron charge, n is the sheet density found from the oscillations period. Fig. 4 is an expanded view of the real part of conductivity σ_1 , shown in Fig. 3, for magnetic fields below 1 T. By drawing the oscillation envelope, it is possible to determine σ_{xx}^* as the average value. Further, by plotting σ_{xx}^* against $1/B^2$, as illustrated in the inset to Fig. 4 for $T=1.6$ K and $f=30$ MHz, one can determine the mobility from the slope of this line as $\mu = 1.5 \times 10^6$ cm 2 /V·s, with $\sigma_{xx}(B=0) = 4.8 \times 10^{-2}$ Ohm $^{-1}$, which are consistent with the results of dc transport measurements on Hall bars taken from the same original wafer. It should be noted that this analysis is only valid in the case where conduction is due to delocalized electrons and the real part of the ac conductivity is equal to the dc value $\sigma_1 = \sigma_{xx}^{dc}$ and does not depend on the frequency of SAW, with $\sigma_2 \approx 0$.

Detailed analysis of the temperature evolution of the conductivity in low fields allows the full set of carrier parameters such as effective mass, Dingle temperature ($T_D \approx 0.6$ K) and quantum relaxation time ($\tau_q \approx 2.2 \times 10^{-12}$ s) to be determined. As these methods are well known from dc transport analysis we will not present the details here, but merely mention the results.

2. Integer Quantum Hall Effect Regime

Let us consider the conductivity mechanisms realized in the IQHE minima with odd filling factor $\nu = 1, 3, 5, 7, 9$. In this case, the charge carriers, electrons, are localized and the high-frequency conductivity has a complex form $\sigma^{ac} = \sigma_1 - i\sigma_2$ which begins to depend on the SAW frequency. In contrast to the low field case, we now have $\sigma_2 > \sigma_1$ and $\sigma^{ac} \neq \sigma_{xx}^{dc}$. This condition arises because the mechanisms of hopping conduction for localized charge carriers are different in ac and dc.⁵ Hence, the existing practice of substituting the dc conductivity in a formula

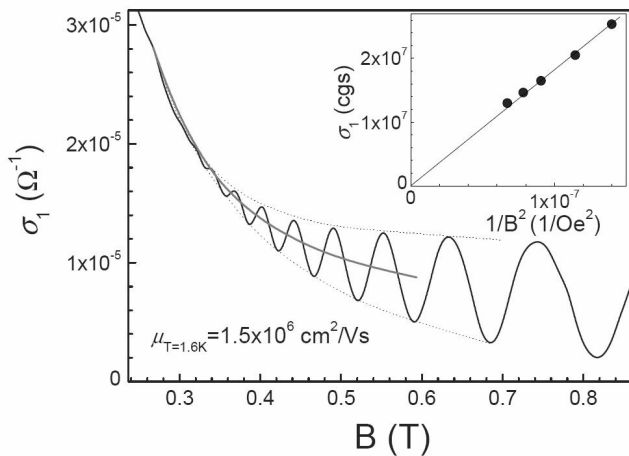


FIG. 4. Magnetic field dependence of the real part of the ac conductivity σ_1 in low fields. The dotted lines are the oscillations envelope; the solid curve is the mean of envelope. Inset: Nonoscillating term of the conductivity σ_{xx}^* vs $1/B^2$; $f=30$ MHz, $T=1.6$ K; line is a result of the linear fit.

like (1) is not valid when localization of carriers takes place in a magnetic field.

Fig. 5 shows how the conductivity for different odd ν , calculated by eqs. (1) and (2), varies with the inverse temperature $1/T$.

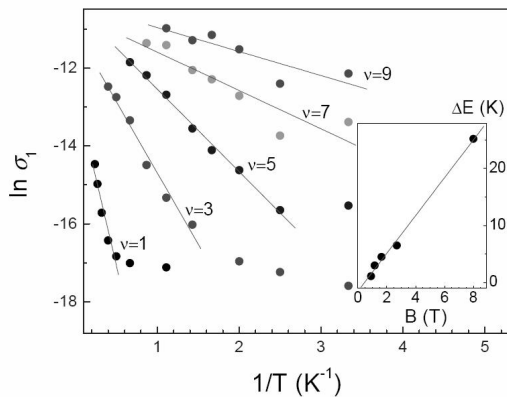


FIG. 5. Arrhenius plot of the real component of the ac conductivity σ_1 at different odd filling factors. Inset: Activation energy in magnetic field for odd filling factors. Lines are results of the linear fit.

Figure 5 demonstrates that at relatively high temperatures all curves show linear dependences on this scale, corresponding to an Arrhenius law $\sigma_1 \propto \exp(\Delta E/2k_B T)$, allowing the activation energy ΔE to be determined. Despite the fact that the change in conductivity is not too large the resulting activation energy $\Delta E \gg k_B T$, so we can use these values in what follows. An activation-like temperature dependence of conductivity is usually associated with electron nearest neighbor hopping in the carrier localization regime. At the low temperature extreme

of Fig. 5 the curves flatten off, which is conventionally attributed to a change of the hopping mechanism. This flattening occurs for all filling factors so is not just an experimental artifact of σ_1 reaching the minimum measurable level. In a high-frequency electric field, the electron hops are between two closely spaced sites (the "two-site" model²⁵), while at dc variable range hopping dominates.

At odd filling factors the activation energy is associated with the formation of spin gaps, so $\Delta E \propto g^* \mu_B B$, (where g^* is the effective g -factor, μ_B is the Bohr magneton). Thus if one plots ΔE against B , as in the inset of Fig. 5, it is possible to determine the g -factor. The slope of the linear dependence gives $g^*=4.9$.

Now let us analyze the frequency dependence of the conductivity. Figure 6 shows the real part of conductivity as a function of SAW frequency on log-log plot to show the power law of this dependence. For $\nu=1$ $\sigma_1 \propto \omega^{1.1}$, and at $\nu=3$ $\sigma_1 \propto \omega^{0.5}$. Thus, for $\nu=1$ $\sigma_1 \propto \omega T^0$. Such a dependence of ac conductivity on temperature and frequency is characteristic of hopping conductivity. This is described by the "two-site" model provided $\omega\tau < 1$, where τ is the time for carriers to hop between energy levels within the pair and $\omega = 2\pi f$ is the SAW frequency. The experimental data show that at high magnetic fields this dependence is well satisfied. The weaker frequency dependence at $\nu=3$ could be explained by assuming that at lower magnetic fields the conduction mechanism is not purely hopping, as not all electrons are localized.

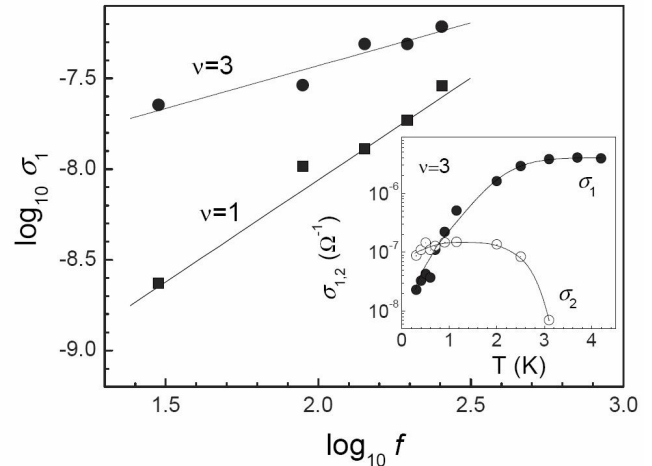


FIG. 6. Dependence of the real component of the ac conductivity σ_1 on frequency at $T=0.3$ K at filling factors $\nu=1$ and 3. Inset: Dependences of the real σ_1 and imaginary σ_2 components of ac conductivity on temperature at filling factor $\nu=3$; $f=30$ MHz. The lines are guides to the eye.

If the complex ac conductivity $\sigma^{ac} = \sigma_1 - i\sigma_2$ has a hopping nature then the imaginary part of the conductivity should exceed the real one, i.e.: $\sigma_2 > \sigma_1$.⁵ This theoretical condition is met as demonstrated in the inset of the Figure 6.

Inset of the Figure 6 shows that at very low temperatures, where carriers are localized and "two-site" hopping

conductivity is realized, $\sigma_2 > \sigma_1$. However, with increasing temperature when the transition to activated conduction occurs σ_1 becomes greater than σ_2 . As the temperature increases the amount of delocalized carriers also increases, driving σ_2 to decrease. Finally, σ_2 becomes vanishing for fully delocalized carriers. It should be noted that in samples with a mobility of 2×10^5 cm²/Vs this ac hopping conduction in the IQHE minima is shunted by a high frequency hopping conductivity via levels of DX-centers.²⁶

3. Regime of the Fractional Quantum Hall Effect at $\nu = 2/3$

Acoustic measurements can also be used to draw conclusions about the conductivity mechanism in the fractional quantum Hall effect regime, by considering the temperature and frequency dependences of the real and imaginary parts of ac conductivity derived from equations (1) and (2). The temperature dependence of both these components for filling factor $\nu=2/3$ are presented in Figure 7, which shows that for $0.3 \text{ K} < T < 0.5 \text{ K}$ σ_1 and σ_2 are the same size whereas at higher temperatures $\sigma_1 \gg \sigma_2 \rightarrow 0$. The inset graph illustrates the dependence of σ_1 on inverse temperature, and provides evidence that activated conductivity takes place in the temperature range from 0.4 K to 1 K. As previously there is a flattening at the low temperature extreme $T < 0.4 \text{ K}$.

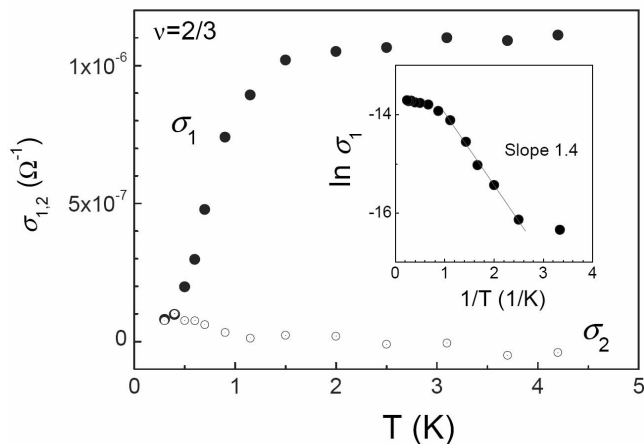


FIG. 7. Dependence of the real σ_1 and imaginary σ_2 components of the ac conductivity on temperature for filling factor $\nu=2/3$. Inset: Arrhenius plot for $\nu=2/3$; $f=30$ MHz.

By varying the SAW frequency, a weak frequency dependence of σ_1 can also be seen at the lowest temperatures measured, which is illustrated in Figure 8. These facts indicate that even at $T=0.3 \text{ K}$, the amount of localized electrons is still small, although the hopping mechanism starts to have an effect on the conductivity.

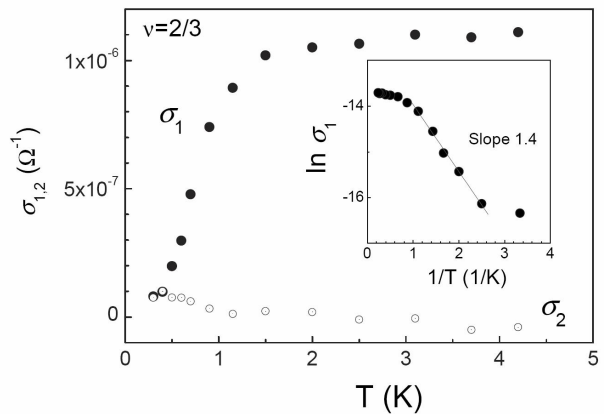


FIG. 8. Frequency dependence of the real component of the ac conductivity for filling factor $\nu=2/3$; $T=0.3 \text{ K}$. The line is guide to the eye.

B. Nonlinear regime

By using larger amplitude surface acoustic waves the non-linear regime can be entered where the response of the 2DEG depends on the SAW intensity. The absorption coefficient Γ and velocity shift $\Delta v/v$ were measured at the base temperature of $T=0.3 \text{ K}$ as a function of the SAW intensity, which was varied from $0.5 \mu\text{W}$ to 5 mW (as measured at the output from the RF generator). We note that the acoustic measurements are carried out in a pulsed mode, so the amount of power being supplied to the 2DEG is negligible and does not simply cause an increase in temperature of the material. This is verified in the experiments, where a sensor mounted on the sample detected no change in sample temperature with SAW application.

The attenuation Γ and velocity shift $\Delta v/v$ in magnetic fields up to 18 T are displayed in Figure 9 at different SAW powers. It is seen that increasing the SAW intensity results in an increase of Γ in all the minima and a decrease of in the maxima of $\Delta v/v$. The following Figure 10 shows the real part of conductivity σ_1 , calculated using the formulas (1 and 2), as a function of the magnetic field at different SAW intensities. Here it is seen that with increasing intensity the ac conductivity in the oscillations minima increases.

The mechanisms of non-linearities that arise with increasing SAW intensity depend on whether the electrons in the 2D channel are localized or delocalized. Therefore we will analyze each conductivity regime separately.

1. Region of delocalized carriers, $B < 1 \text{ T}$

The high electric field of the intense SAW field leads to heating of the free charge carriers (Ref. 27 and references therein). In this case, one can introduce the concept of an electron temperature T_e , which is above the lattice temperature T_p . Then T_e can be determined by compar-

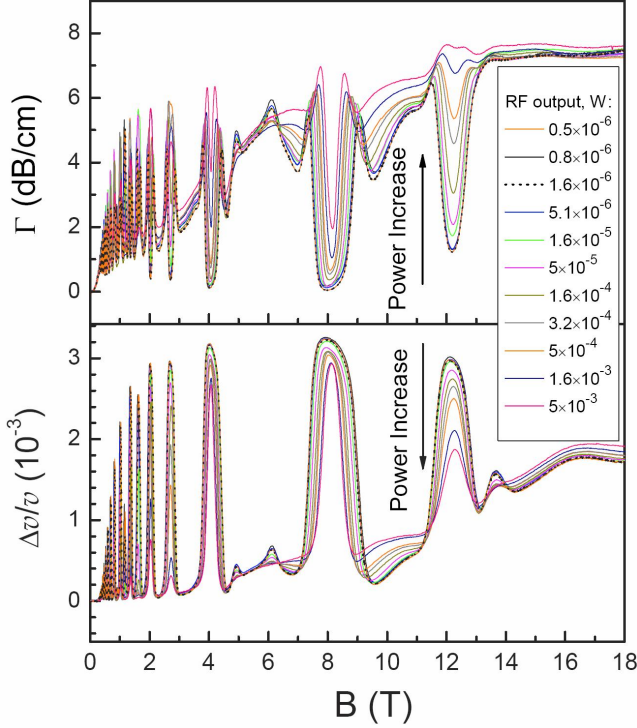


FIG. 9. (Color online) Power evolution of the ultrasound attenuation Γ and relative change of velocity $\Delta v/v(0)$ dependences on the magnetic field; $f = 30$ MHz, $T=0.3$ K.

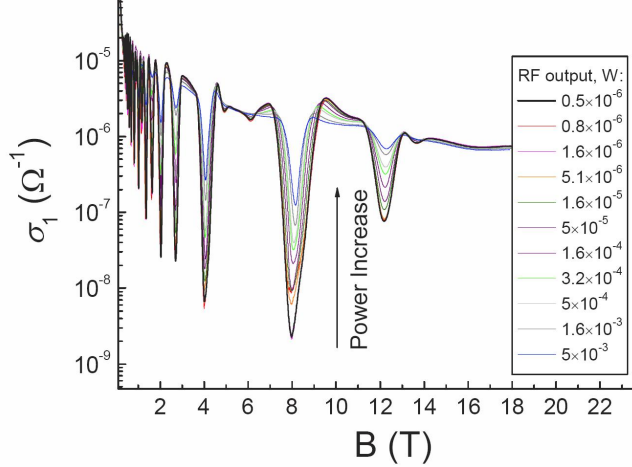


FIG. 10. (Color online) Dependence of the real part of the ac conductivity on magnetic field at different SAW intensities; $T=0.3$ K.

ing the dependence of Γ on lattice temperature measured in linear regime with the dependence of Γ on the SAW intensity measured at the lowest temperature.

The condition for introducing a carrier temperature is

$$\tau_p \ll \tau_{ee} \ll \tau_\varepsilon, \quad (4)$$

where τ_p , τ_{ee} , and τ_ε are the momentum, electron-electron, and energy relaxation times, respectively.

The electron-electron relaxation time is given by

$$\frac{\hbar}{\tau_{ee}} = \frac{k_B T \rho e^2}{h} \ln \frac{h}{2e^2 \rho}, \rho = 1/\sigma. \quad (5)$$

which leads to a value of $\tau_{ee} = 5 \times 10^{-9}$ s. The momentum relaxation time has been found from the mobility at $T=1.6$ K $\tau_p = 6 \times 10^{-11}$ s.

As regards the energy relaxation time, its calculation will be discussed later.

To determine the absolute energy loss rate $Q = e\mu E^2$ per electron, it is necessary to know the electric field which accompanies the SAW. This value is determined by the formula²⁷ (if $\sigma_2 = 0$):

$$|E|^2 = K^2 \frac{32\pi}{v} \frac{(\varepsilon_1 + \varepsilon_0)zqe^{(-2q(a+d))}}{[1 + (\frac{4\pi\sigma_1(\omega)}{\varepsilon_s v}t(q))^2]} W, \quad (6)$$

$$z(q) = [(\varepsilon_1 + \varepsilon_0)(\varepsilon_s + \varepsilon_0) - (\varepsilon_1 - \varepsilon_0)(\varepsilon_s - \varepsilon_0)e^{-2qa}]^{-2},$$

where W is the input SAW power scaled to the width of the sound track.

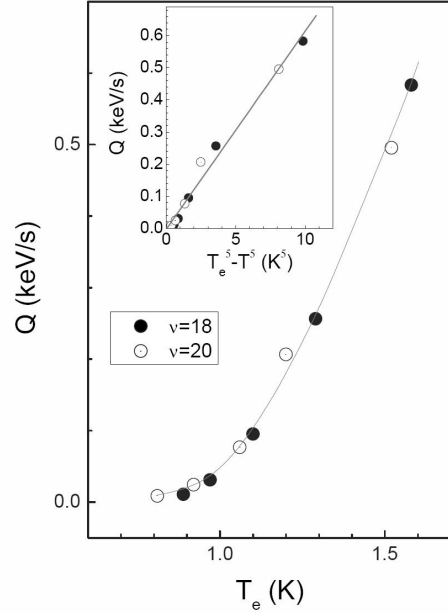


FIG. 11. The energy losses rate per electron versus T_e ; $T=0.3$ K, $f=30$ MHz. The line is guide to the eye. Inset: dependence of Q on $(T_e^\gamma - T^\gamma)$, $\gamma = 5$. Line is the result of the linear fit.

The variation of Q with T_e obtained from the experimental results is shown in Fig. 11 and could be well fitted by the functional form $Q = A_5(T_e^5 - T^5)$, which corresponds to energy relaxation via carrier scattering from the piezoelectric potential of the acoustic phonons (PA-scattering) with strong screening.

The value of A_5 , found from the slope of the dependence $Q = A_5(T_e^5 - T^5)$, is $A_5 \approx 62$ eV/sK⁵ (the

theoretical calculation using the piezoelectric constant $\beta_{14} = 3.6 \times 10^4$ cgs gives $A_5 = 92$ eV/sK⁵)²⁸. The value of the energy relaxation time τ_ε can be determined using the equation for arbitrary heating²⁹:

$$\tau_\varepsilon = \frac{\pi^2 k_B^2 (T_e^2 - T^2)}{6 E_F A_5 (T_e^5 - T^5)}. \quad (7)$$

where E_F is the Fermi energy. The energy relaxation time calculated with known A_5 and Eq. 7 depends on T_e , but for low heating $\Delta T_e \ll T$ $\tau_\varepsilon \approx 5 \times 10^{-7}$ s and the condition $\omega \tau_\varepsilon \gg 1$ is easily satisfied. This means that the energy relaxation time is much greater than the period of the SAW oscillations and so the heating processes depend on the time averaged SAW intensity.

Thus, relation (4) is also satisfied which allows us to explain the observed nonlinear effects in the delocalized electrons region as simply the heating of free electrons by the electric field of the SAW.

2. Integer Quantum Hall Effect Regime

The presence of charged impurities leads to random fluctuations in the electrostatic potential of the 2DEG and means that electrons have to be excited to a percolation level for conduction to occur. The influence of a strong static electric field on this activated conductivity was considered theoretically in Ref. 30 and shown to decrease the activation energy, which can be interpreted as a lowering of the percolation threshold. For the two dimensional case, the dependence of the conductivity on electric field will look like:

$$\sigma_1 = \sigma_1^0 \exp(\alpha E^{3/7} / k_B T), \alpha = (C e l_{sp} V_0)^{3/7}. \quad (8)$$

where σ_1^0 is the conductivity in the linear regime, l_{sp} is the spatial scale of the potential variation, which for modulation doped heterostructures could be counted as equal to the spacer width, and V_0 is the random fluctuation potential amplitude.

In our experiment, when the condition $\omega \tau_p \ll 1$ is valid, the wave (SAW) can be considered as stiffened, so to interpret the nonlinear effects in the ac conductivity one may to apply a theory obtained for the strong static electric field. Although, we studied nonlinear effects at $T = 0.3$ K, where the conductivity no longer has an activation character, but was very weakly dependent on temperature (as expected for the case of two-site hopping), the dependence of the real conductivity σ_1 on the electric field of surface acoustic wave shown in Figure 12 is nevertheless well described by the dependence $\ln \sigma_1 \propto E^{3/7}$ predicted by equation (8). One can assume that the nonlinearity mechanism is complex: simply heating the electrons in an electric field of the SAW leads to the activated dependence of conductivity on temperature, the nonlinearity in this case is characterized by nonlinear conduction at the percolation level, as in Ref. 30.

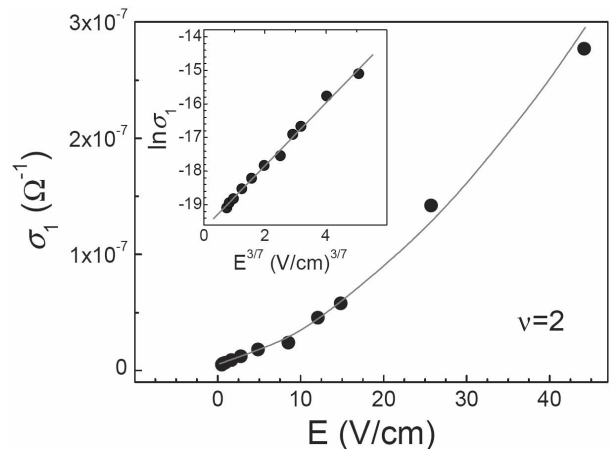


FIG. 12. Variation of the real component of the ac conductivity with the SAW electric field for $\nu=2$; $f=30$ MHz, $T=0.3$ K. Inset: $\ln \sigma_1$ vs $E^{3/7}$. Line is a result of the linear fit.

3. Fractional Quantum Hall Effect Regime

All that was said about the nonlinear effects in σ_1 in the previous section for $\nu=2$, is fully applicable to σ_1 in the minimum of oscillations at $\nu=2/3$, but with a much larger reason because activated conductivity for this case remains practically down to $T=0.3$ K. Indeed Fig. 13 very clearly demonstrates that the $\ln \sigma_1 \propto E^{3/7}$ law is valid for the experiment at $\nu=2/3$.

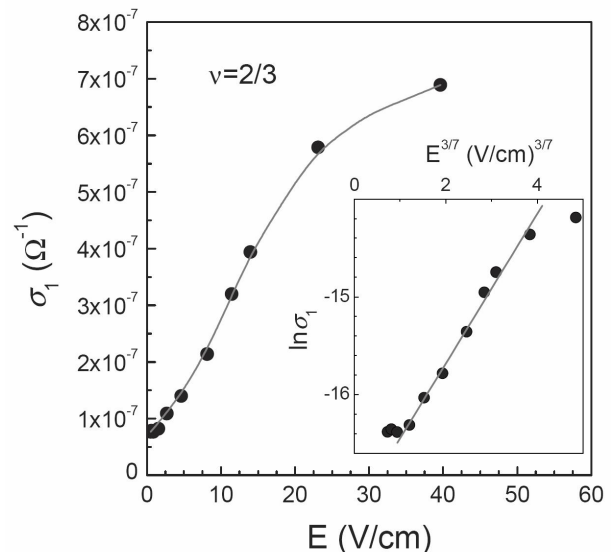


FIG. 13. Dependence of the real component of the ac conductivity on the SAW electric field E . Inset: $\ln \sigma_1$ on $E^{3/7}$; $\nu=2/3$. Line is a result of the linear fit.

C. Conductivity in a tilted magnetic field

It is well known that in the fractional quantum Hall effect regime at $\nu=2/3$ the spin polarized-unpolarized phase transition occurs with changes of concentration or magnetic field.^{11–14} Keeping in mind the description of the FQHE many-body ground state as a one-electron state of composite fermions, the $\nu=2/3$ FQHE state translates into the $\nu=2$ IQHE state of composite fermions. In this case, the spin transition occurs due to crossing of CF LLs with different spin direction as the magnetic field or concentration changes. This transition has been investigated in numerous papers and by different experimental methods. As the concentration of our sample was $n = 2 \times 10^{11} \text{ cm}^{-2}$ we could not explore this transition directly, since the $\nu=2/3$ state in our experiment was at $B=12$ T, while the spin transition occurs at lower magnetic fields. So we could merely investigate the fully spin-polarized state. The usual routine in this case is to study the activation energy of conductivity in a tilted magnetic field, which for $\nu=2/3$ in the fully spin-polarized state has been done using various methods.^{11–14,17–20} However, the functional form reported for this dependence varies from $\Delta E \propto B^1$ (Ref. 17, 20) to a sublinear one with a saturation.^{11,18}

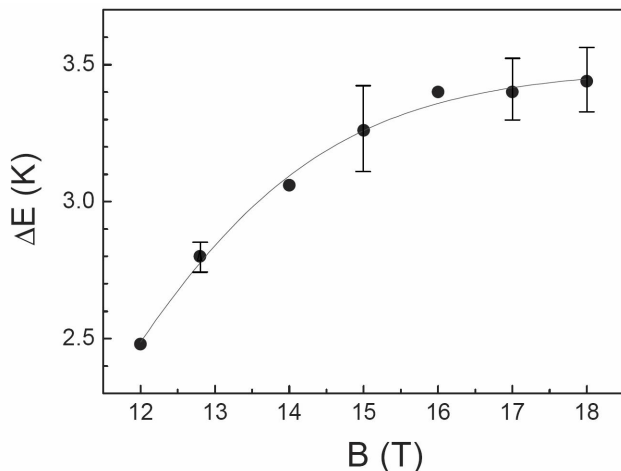


FIG. 14. Dependence of the activation energy ΔE on magnetic field for $\nu=2/3$; $f=30$ MHz. The line is guide to the eye.

Tilting the magnetic field relative to a normal to the sample surface enabled us to change the position of the conductivity minimum at $\nu=2/3$ from $B=12.0$ T up to $B=17.8$ T. We measured the temperature dependence of Γ and $\Delta v/v$ in the range of 0.4 K to 1.6 K for each tilt angle and calculated σ_1 using formulas (1) and (2). The activation energy ΔE was derived by constructing the Arrhenius plot $\ln \sigma_1$ against $1/T$ and the resulting dependence of ΔE on magnetic field is illustrated in Fig. 14.

It has been predicted, that in the FQHE regime the energy difference between Landau levels $\Delta E \propto B^{1/2}$. However, as in all the previously cited works, our data shows

that such dependence is not obeyed. The reason for this is firstly that the method of determining ΔE from the temperature dependence of conductivity minima leads one to determine an activation energy to the mobility edge: the value of which will differ from the value of the gap in the Landau levels spectrum by the width of the region of delocalized states. In order to obtain the actual gap between LL centers one can instead apply the Lifshitz-Kosevich (LK) formula to the damping of the SdH oscillations with temperature.^{15,16} In Ref. 16 it was found that the energy gap between centres of the spin polarised CF Landau levels does scale with the effective magnetic field seen by the composite fermions and in Ref. 16 it was shown that changing the effective g-factor through application of hydrostatic pressure has no effect on the gap of a polarized state at $2/3$. Secondly, tilting the field also changes the in-plane component of magnetic field which serves to compress the wavefunction closer to the interface, as modeled in Ref. 31, and leads to deviations from the simple square root behavior.

Nevertheless, it can be seen that acoustic techniques provide a contact-free method of obtaining the information more usually sought from dc transport experiments and are probing the similar physics, with the same limitations. In principle, the LK formula could also be applied to the acoustic results, but we are reluctant to do so with the current data set since the oscillations are far from sinusoidal.

IV. CONCLUSION

In this paper we have demonstrated a method to determine the complex high frequency conductivity in an n -GaAs/AlGaAs heterostructure using acoustic contactless techniques in a "hybrid" geometry.

This work has shown that, in a structure exhibiting the quantum Hall effect, one can separate the regions of delocalized and localized electrons through application of a magnetic field.

At low magnetic fields, $B < 1$ T, electrons are delocalized thus one can determine the general parameters of the two-dimensional electron gas using contactless acoustic methods: concentration, mobility, Dingle temperature, and the transport, quantum and energy relaxation times. The method is powerful and clearly justified since the parameters determined by acoustic methods coincide to within 10% of those measured by direct current.⁴ At higher fields, the mechanisms of low temperature high frequency conductivity have been analyzed in the IQHE oscillations minima, and shown to be predominately by hopping, which is well explained by the "two-site" model.

In the fractional quantum Hall effect regime at $\nu=2/3$ the conductivity has an activation character. The dependence of the activation energy on magnetic field has been determined and shown to follow a similar trend to measurements by other techniques.

A major feature of using this acoustic technique is that

all the conductivity measurements can be made without needing to fabricate contacts. We expect this to be most desirable in evaluating emerging novel material systems where the fabrication technology and surface interactions are less well understood.

A. Acknowledgments

The authors are grateful to Yu.M. Galperin for useful discussions and thank E. Palm, T. Murphy, J.H. Park, and G. Jones for help with the experiments. The authors also thank J.J. Harris and C.T. Foxon for growing the sample G157 back in 1986 and see this work as excellent evidence of the longevity of their GaAs material. This work was supported by grant of RFBR 11-02-00223, a grant of the Presidium of the Russian Academy of Science, the Program "Spintronika" of Branch of Physical Sciences of RAS. The NHMFL is supported by the NSF through Cooperative Agreement No. DMR-0654118, the State of Florida, and the DOE.

-
- * ivan.smirnov@mail.ioffe.ru
- ¹ *The Quantum Hall effect*, edited by R.E. Prange and S.M. Girvin (Springer-Verlag, New-York 1987).
 - ² A. Wixforth, J.P. Kotthaus, and G. Weimann, *Phys. Rev. Lett.* **56**, 2104 (1986).
 - ³ A.L. Efros, and Yu.M. Galperin, *Phys. Rev. Lett.* **64**, 1959 (1990); V.D. Kagan, *Fiz. Tekh. Poluprov.* **31**, 478 (1997); *Semiconductors* **31**, 407 (1997).
 - ⁴ I.L. Drichko, A.M. Diakonov, E.V. Lebedeva, I.Yu. Smirnov, O.A. Mironov, M. Kummer, and H. von Känel, *J. Appl. Phys.* **106**, 094305 (2009).
 - ⁵ A.L. Efros, *Zh. Eksp. Teor. Fiz.* **89**, 1834 (1985); *JETP* **89**, 1057 (1985).
 - ⁶ I.L. Drichko, A.M. Diakonov, I.Yu. Smirnov, Y.M. Galperin, and A.I. Toropov, *Phys. Rev. B* **62**, 7470 (2000).
 - ⁷ For reviews, see articles in *Perspectives in Quantum Hall Effect*, edited by S. Das Sarma and A. Pinczuk (Wiley, New York, 1996).
 - ⁸ R.L. Willett, *Adv. Phys.* **46**, 447 (1997).
 - ⁹ B.I. Halperin, P.A. Lee, and N. Read, *Phys. Rev. B* **47**, 7312 (1993).
 - ¹⁰ I.V. Kukushkin, J.H. Smet, V.W. Scarola, V. Umansky, and K. von Klitzing, *Science* **324**, 1044 (2009).
 - ¹¹ J.P. Eisenstein, H.L. Stormer, L.N. Pfeiffer, and K.W. West, *Phys. Rev. B* **41**, 7910 (1990).
 - ¹² L.W. Engel, S.W. Hwang, T. Sajoto, D.C. Tsui, and M. Shayegan, *Phys. Rev. B* **45**, 3418 (1992)
 - ¹³ O. Stern, Ph.D. thesis, Max Planck Institute, Stuttgart, 2004.
 - ¹⁴ R.G. Clark, S.R. Haynes, J.V. Branch, A.M. Suckling, P.A. Wright, P.M.W. Oswald, J.J. Harris, and C.T. Foxon, *Sur. Sci.* **229**, 25 (1990).
 - ¹⁵ R.J. Nicholas, D.R. Leadley, M.S. Daly, M. van der Burgt, P. Gee, J. Singleton, D.K. Maude, J.C. Portal, J.J. Harris and C.T. Foxon, *Semicond. Sci. and Technol.* **11**, 1477 (1996).
 - ¹⁶ D.R. Leadley, R.J. Nicholas, D.K. Maude, A.N. Utjuzh, J.C. Portal, J.J. Harris and C.T. Foxon, *Phys. Rev. Lett.* **79**, 4246 (1997).
 - ¹⁷ F. Schulze-Wischeler, E. Mariani, F. Hohls, and R.J. Haug, *Phys. Rev. Lett.* **92**, 156401 (2004).
 - ¹⁸ R.J. Haug, K. v. Klitzing, R.J. Nicholas, J.C. Maan, and G. Weimann, *Phys. Rev. B* **36**, 4528 (1987).
 - ¹⁹ G.S. Boebinger, H.L. Stormer, D.C. Tsui, A.M. Chang, J.C.M. Hwang, A.Y. Cho, C.W. Tu, and G. Weimann, *Phys. Rev. B* **36**, 7919 (1987)
 - ²⁰ V.S. Khrapai, A.A. Shashkin, M.G. Trokina, V.T. Dolgoplov, V. Pellegrini, F. Beltram, G. Biasiol, and L. Sorba, *Phys. Rev. Lett.* **99**, 086802 (2007).
 - ²¹ D.R. Leadley, R.J. Nicholas, P.J. Gee, J. Singleton, J.J. Harris and C.T. Foxon, in *Proceedings of the 22nd International Conference on the Physics of Semiconductors, Vancouver, 1994*, edited by D.J. Lockwood (World Scientific, Singapore, 1995), Vol. 3, p. 983.
 - ²² D. Dini, R.B. Dunford, O. Stern, W. Dietsche, C.J. Mellor, K. von Klitzing, and W. Wegscheider, *Phys. Rev. B* **75**, 153307 (2007).
 - ²³ J.J. Harris, C.T. Foxon, K.W.J. Barnham, D.E. Lacklison, J. Hewett, and C. White, *J. Appl. Phys.* **61**, 1219 (1987).
 - ²⁴ T. Ando, *J. Phys. Soc. Japan* **37**, 1233 (1974).
 - ²⁵ M. Pollak and T. Geballe, *Phys. Rev.* **122**, 1742 (1961); Yu.M. Galperin, V.L. Gurevich, and D.A. Parshin, in *Hopping Transport in Solid*, edited by B. Shklovskii and M. Pollak (Elsevier, New York 1991).
 - ²⁶ I.L. Drichko, A.M. D'yakonov, I.Yu. Smirnov, Yu.M. Gal'perin, V.V. Preobrazhenskii, and A.I. Toropov, *Fiz. Tekh. Poluprov.* **38**, 729 (2004); *Semiconductors* **38**, 702 (2004).
 - ²⁷ I.L. Drichko, A.M. D'yakonov, V.D. Kagan, A.M. Kreshchuk, T.A. Polyanskaya, I.G. Savel'ev, I.Yu. Smirnov and A.V. Suslov, *Fiz. Tekh. Poluprov.* **31**, 1357 (1997); *Semiconductors* **31**, 1170 (1997).
 - ²⁸ V. Karpus, *Fiz. Tekh. Poluprov.* **22**, 439 (1988); *Sov. Phys. Semicond.* **22**, 268 (1988).
 - ²⁹ V.F. Gantmakher and Y.B. Levinson, *Carrier scattering in metals and semiconductors* (North-Holland, Amsterdam 1987).
 - ³⁰ B.I. Shklovskii, *Fiz. Tekh. Poluprov.* **13**, 93 (1979); *Sov. Phys. Semicond.* **13**, 53 (1979).
 - ³¹ P.J. Gee, F.M. Peeters, J. Singleton, S. Uji, H. Aoki, C.T.B. Foxon, and J.J. Harris, *Phys. Rev. B* **54**, R14313 (1996).